Faculty of Natural Science and Technology
Department of Physics

NTNU
Innovation and Creativity

PROJECT THESIS FOR

STUD. TECHN. ANDERS LUND EIDE

Thesis started:	16.02.2009
Thesis submitted:	20.08.2009

DISCIPLINE: TECHNICAL PHYSICS

Norsk tittel: *"Optikk utvikling for resirkulerende elektron linac i en høyenergetisk hadron-lepton kollisjonør (LHeC) ved LHC"*

English title: *"Optics development for the recirculating electron linac of a high-energy hadron-lepton collider (LHeC) at the LHC"*

This work has been carried out at CERN, under the supervision of Frank Zimmermann. Bo-Sture Skagerstam has been the responsible supervisor from the Department of Physics.

Abstract

This report discusses the beam optics of several electron linac options for a high-energy hadron-lepton collider (LHeC) based on the LHC and is part of undergoing feasibility studies for this project. The report provides a proof of principle that a high luminosity and energy LHeC based on a linac is possible and lattice designs for recirculating electron linacs, both with and without energy recovery, is suggested for several energies. In particular the betatron and dispersion functions of these designs are discussed.

Preface

This project work was done the spring 2009 as a part of the master's degree program in Technical Physics at the Norwegian University of Science and Technology. The course code of the Specialization Project is TFY4510, and the course amounts to 15 ECTS-credits. To support the work there has been a local supervisor from CERN, Frank Zimmermann, and a supervisor from NTNU, Bo-Sture Skagerstam.

Most of my working time during this semester has been spent on this project, and it has been a challenge to put so much focus on one single project. I am nevertheless very satisfied that I got the opportunity to give a small contribution to the designing of a new particle accelerator and to learn about particle accelerator physics where it is actually done.

Contents

List of Figures

Chapter 1

Introduction

This chapter will in a concise manner explain the background for the work presented in this report. CERN and the Large Hadron-electron Collider (LHeC), with both its design options, will be presented, and the physics motivation for studying lepton-hadron collisions, e.g. deep inelatsic scattering, at this energy scale will be briefly discussed. In addition a very short introduction to beam optics is given.

1.1 CERN

CERN is the worlds largest particle physics laboratory and is located near Geneva in Switzerland. It was founded in 1954 and has been responsable for some of the most important discoveries in subatomic physics in the last demi-siecle (e.g. the Z and W bosons, and direct CP-violation). Today much of the activity at CERN is focused on the Large Hadron Collider (LHC), but planes are already being made for future projects, although this will also depend on the results from LHC. One of the post-LHC projects under concideration (that involves the LHC itself and will thus extend the productive lifetime of this great machine) is the LHeC.

1.2 LHeC: The Large Hadron-electron Collider

A proton-electron collider at TeV-scale energies based on the LHC and the Large Electron-Positron Collider (LEP) accelerators was first suggested by F. Close as early as in 1990 [2]. However the proposal has several times undergone large changes since its birth. LEP is no longer a candidate for the electron acceleration and is already dismantled, and a new electron accelerator is thus needed for the realization of this project. Two different accelerator types are considered – a storage ring and a linear accelerator (linac). Both of these options are to be developed in a conceptual design report to be finished in 2010 under a mandate of ECFA [1]. The work presented in this report has focused on the electron accelerator design for the linac option.

For the experiments to be performed by the LHeC there are two important machine parameters. The center of mass energy and the luminosity in the collisions. The center of mass energy m_{cm} is given by

$$m_{cm} = (P_p^\mu + P_e^\mu)(P_{p,\mu} + P_{e,\mu}) = \sqrt{(E_p + E_e)^2 - (\mathbf{p}_p + \mathbf{p}_e)^2} \approx 2\sqrt{E_p E_e}. \quad (1.1)$$

The subindices p and e refer to proton or electron, E indicates the energy of the respective particles, $\mathbf{p}$ the momentum and P^μ the four momentum ($P^\mu P_\mu$ is

Lorentz invariant). The luminosity L is found from

$$L = \frac{1}{4\pi e}\frac{N_{b,p}}{\epsilon_p}\frac{1}{\beta_p^*} I_e H_{hg}(\frac{\beta_e^*}{\sigma_{z,p}}, \frac{\epsilon_e}{\epsilon_p}). \tag{1.2}$$

where e denotes the electron charge and the subindices are as before. The luminosity depends on the number of particles per bunch $N_{b,p}$, the geometric emittance ϵ_p and the interaction point β-function β_p^* of the proton beam, the current I_e of the electron beam, and the hourglass factor H_{hg} (see reference) [4]. A comparison of the luminosity and energy for the different options are shown in figure 1.1.

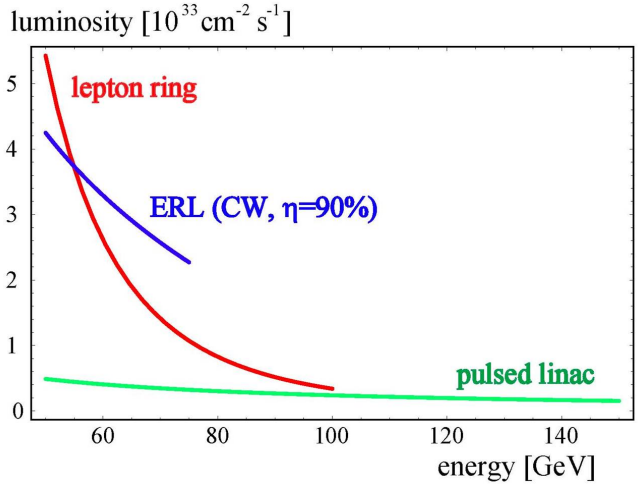

Figure 1.1: The luminosity as a function of energy for three LHeC options with 100 MW electrical power for the purpose of illustration. The efficiency of the energy recovery is taken to be 90% for the ERL (from [5]).

1.2.1 Particle physics motivation

The Standard Model of Particle Physics (SM) has been and is a remarkably successful theory. However, it is known to be incomplete and fails to account for some unignorable physical phenomenas (e.g. dark matter). Several complementing theories have been suggested to solve this problem, but, as data from experiments at sufficiently high energies is not available, none of these have so far been proven either plausible or incorrect. The LHC , scheduled to restart in November of this year is hoped to alter this, but, although it might indeed provide answers to some questions (and among other things hopefully prove the existence of the Higgs boson), it will certainly be less well suited to answer others. And it might give only an indication of the existence of other phenomena, but little information about their character, so that they will need to be studied further in a different machine type. This is where LHeC comes in. Although it is in general unlikely that a discovery at the LHeC will be invisible at the LHC, the LHeC might be needed to study further a phenomenon found at the LHC. Possible examples of LHC discoveries that might prompt the building of the LHeC are leptoquarks (i.e. lepton–quark resonances), new leptons (e.g. sleptons) and new Z′ bosons. The LHeC might also be needed to provide a better knowledge about the proton structure that could be needed to better study new bosons or to unambiguously establish new physics effects with the LHC, and in general to allow for high precision physics with LHC proton–proton collisions. It does seem clear that the motivation to build the LHeC

is strong enough will depend heavily on the findings of the LHC [6, 7, 13]. The energy one would want in such a machine does also depend on the results from the LHC, although there is strong political arguments for a center of mass energy above 1 TeV. From (1.1) we find that with 7 TeV proton energy this requires an electron energy of at least 36 GeV.

Historic perspective

A decade ago three different types of particle accelerators were operating in center of mass energies of about the same order of magnitude (i.e. of several hundred GeVs). The LEP and the SLAC linac were producing electron–positron collisions, Tevatron proton–anti-proton collisions, and HERA (Hadron Elektron Ringanlage) electron–hadron collisions, and each of these were providing valuable data and the machines complemented each other. The LHC will now bring particle physics into the terascale (i.e. the TeV energy scale) and replace the Tevatron as the largest and most awesome hadron collider in the world, but what machines, if any, that are to take the place of HERA or LEP is not yet clear. There are two proposals for a terascale electron–positron collider, the International Linear Collider (ILC) and the Compact Linear Collider (CLIC). Both of these projects are in the planing stage, the ILC having come out with a design report two years ago and CLIC hoping to do so next year, and will at the earliest start construction in 2015. For a terascale lepton–hadron collider the LHeC is currently the only project in active development (the THERA project now being abandoned) and a conceptual design report (covering both electron accelerator option) is to be finished by the end of this year or early in 2010. An overview of planned and proposed lepton–hadron colliders is shown in figure 1.2.

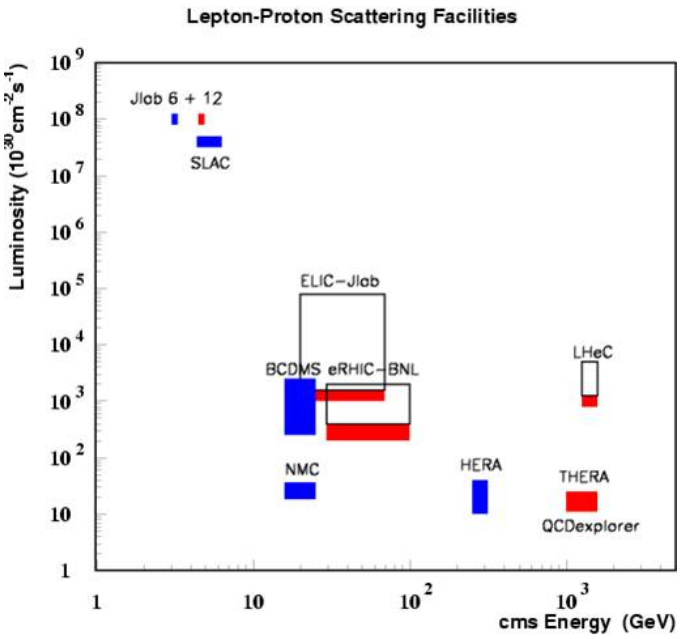

Figure 1.2: Summary of existing (blue boxes) and proposed (red boxes) facilities for lepton–proton deep-inelastic scattering investigations in terms of the luminosity and centre-of mass energy (from [6]).

1.2.2 The ring-ring option

Although the rest of this report will not deal with the ring-ring option a very concise evaluation of the advantages and disadvantages should be of interest. A storage ring may require less R&D than a linac would, because such a machine has already been built and run, at even higher energies than what is currently projected forLHeC, namely the LEP. However the LHeC would have significantly higher electron beam current [5]. There is also a change in the geometry from the LEP ring caused by the need for the new ring to bypass the LHC experiments. This difficulty is possible to overcome, although one might potentially encounter new problems and the necessary extension of the tunnel could be particularly challenging in some areas (e.g. because of an underground river) [20]. Other challenges are the need for an injector for the electron storage-ring and the need for proton crab-cavities to be installed in LHC. It will also be extremely difficult or impossible to provide polarized electrons at energies above 50 GeV, a requirement in some of the future LHeC experiments. In general a storage ring has the advantage over a linac that the accelerating cavities are used many times to accelerate each particle, something that reduces both the construction and the operational costs. Although a storage ring will give loss of beam power due to synchrotron radiation the power you save by passing the particles through the cavities many times, outweighs this (at the projected energy) and makes it possible to have higher beam current, resulting in higher luminosity. A serious drawback with the ring-ring option is that synchrotron radiation limits the energy to about 70GeV, or certainly to less than 100 GeV, the maximum LEP energy. Another drawback is the necessity of closing the LHC for the duration of the construction period, whereas for the linac option LHC probably only needs to be closed for a short period during the work in the LHeC interaction region and its proximity. An overview of the layout for the ring-ring option is shown in figure 1.3.

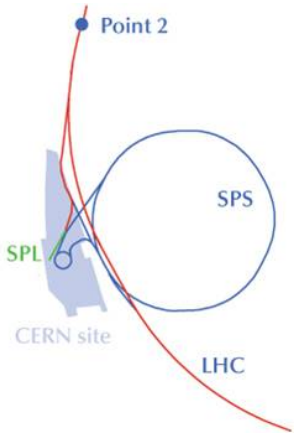

Figure 1.3: A schematic view of the proposed LHeC ring-ring layout. The Superconducting Proton Linac (SPL), part of the Super LHC (SLHC) upgrade, is here suggested used for injection to the storage ring (from [5]).

1.2.3 The ring-linac option(s)

The ring-linac option originates from the idea of constructing either the Compact Linear Collider (CLIC) or the International Linear Collider (ILC) tangentialy to LHC and extract leptons for deep-inelastic scattering with LHC protons. Although recent studies have shown this to be impracticable [20], the ring-linac option for

LHeC, now with a dedicated electron linac, has survived. There will obviously be important synergies between the development of an LHeC linac and other future linac projects, and it might even be possible to reuse certain components from LHeC for a larger machine.

Apart from the use of forward looking technology other advantages of the linac option are the possibility of going to higher energies, constructing the machine in steps (i.e. upgrading to higher energy after the first years of operation), the possibility of reaching a much lower emittance and of obtaining a high electron polarization. Drawbacks when comparing with the ring-ring option are the lower luminosity (at least without energy recovery), possibly higher construction costs (because of the need for much more RF-cavities) and a bigger challenge in positron production [5].

A possibility of reducing the high construction cost of a linac is provided by the option of making it recirculating. This way one can use the same accelerating cavities several times, thereby reducing the length of the linac by a factor equal to the number of circulations chosen. This does however create some losses to synchrotron radiation, similarly to a storage ring, and the number of recirculations needs to be optimized. Studies for LHeC by Jake Skrabacz have shown that the cost optimum for a machine with beam energy between 60 and 140 GeV is one recirculation, i.e. two passes through the linac [17].

To conteract the lower luminosity of the linac option (arrising from the limited beam current) one has to reduce the power needed to accelerate a particle to the desired energy such that the number of particles one can bring to this energy for a given wall-plug power input is increased. An elegant way of doing this is using an Energy-Recovery Linac (ERL). This relatively newly developed machine type, the first was successfully commissioned at the Thomas Jefferson National Accelerator Facility (JLAB) in 1999, recovers the energy from the beam by decelerating after the collision (or whatever other use the beam is put to, at JLAB the ERL was used as a Free-Electron Laser (FEL)). This is done either with two linacs facing each other, accelerating in one and decelerating in the other, or by circulating the beam, passing it through the same cavities again with a phase shift causing it to see a decelerating rather than accelerating field. In an ERL it might also be possible to recover and reuse particles from the beam, thereby making the supply of positrons easier. It does however have a technical drawback in addition to the increased cost and difficulty of the construction. To either recirculate the particles or pass them on to an opposing linac for deceleration it will probably be necessary to operate in continuous wave mode, i.e. the accelerating cavities are always filled with the standing electromagnetic wave used to accelerate the particles, rather than the pulsed mode one would otherwise use. To be able to sustain the extremely low temperature needed in the super-conducting RF-cavities, at reasonable costs for electrical power, the accelerating gradient must be reduced, resulting in an increase of the length of the linac and/or a reduction of the energy of the machine. It is therefore not at all obvious that the ERL option should be the final ring-linac proposal.

In this paper three different accelerators are considered. A recirculating linac with two passes and 100 GeV collision energy, a recirculating linac (RL) with two passes and 140 GeV collision energy, and an ERL with two passes for acceleration and two for deceleration with 60 GeV collision energy. A suggestion for geometry and placement of the ring-linac LHeC is shown in figure 1.4.

1.3 Beam optics – central concepts and terminology

In particle accelerators we use magnetic fields to guide charged particles along a predescribed path, or at least keep them close by. This path, called the reference

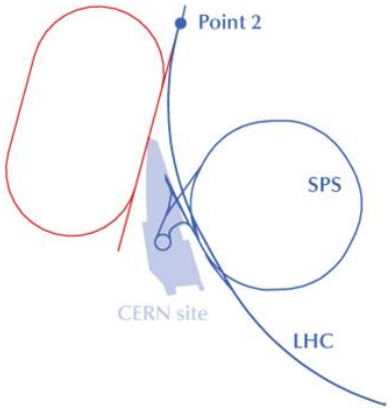

Figure 1.4: A schematic view of the proposed LHeC ring-linac layout with a race-track design recirculating linac (from [5]).

trajectory, is defined geometrically by straight sections and bending magnets (i.e. dipoles) only. A particle following the reference trajectory is called ideal particle. To keep particles, with slightly different position or momentum from the ideal particle, close to the reference trajectory we use focusing magnets (i.e. quadrupoles; we disregard other focusing effects for now) that are arranged in a periodic lattice. The lattice consists of smaller segments called cells with only a few magnets, that are placed in sequence over the entire beam line. The most simple and realistic periodic lattice is formed by cells of alternating focusing and defocusing quadrupoles. This focusing structure is called a FODO-cell and is shown in figure 1.5.

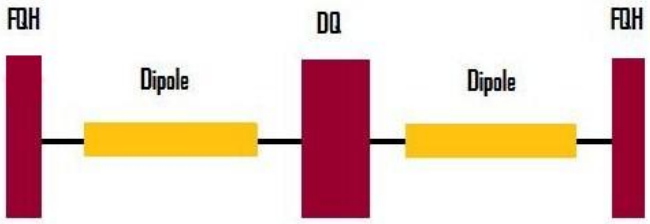

Figure 1.5: Schematic drawing of a FODO-cell with dipoles (not to scale). FQH signifies half of a focusing quadrupole (focusing in the horizontal plane), DQ signifies a quadrupole defocusing in the same plane. In the straight part of an accelerator the dipoles will be replaced by drift spaces or, in a linac, RF-cavities.

The equation of motion of a particle through a lattice can be solved analytically. The differential equation of motion is

$$u'' + k(s)u = 0, \tag{1.3}$$

where u stands for x or y (i.e. the deviation from the reference trajectory in the horizontal or vertical plane) and $k(s)$ describes the focusing at a particular position s in the lattice. We use an ansatz with an s-dependent amplitude β and phase ψ

$$u(s) = a\sqrt{\beta(s)}cos[\psi(s) - \psi_0], \tag{1.4}$$

where the quantities a and ψ_0 are integration constants. A specific normalization is chosen for the phase function such that we have

$$\psi(s) = \int_0^s \frac{dt}{\beta(t)} + \psi_0. \tag{1.5}$$

When we concider the change in phase between two positions we often speek of the phase advance of the structure. $\beta(s)$ is known as the betatron- or β-function and, as it is proportional to the size of the beam in any given position, its development through the lattice is one of the first things to concider when evaluating a new design. It is one of the so called twiss parameters, the others being $\alpha = -\beta'/2$ and $\gamma = (1-\alpha^2)/\beta$, that are parameters in a constant of motion obtained from (1.4) called the Courant-Snyder invariant and given by

$$\gamma u^2 + 2\alpha u u' + \beta u'^2 = a^2 =\leq \epsilon. \tag{1.6}$$

This invariant expression is equal to the equation of an ellipse with the area πa^2 which describes the trajectory of a single particle in phase space. Although the form of the ellipse is changing constantly, any particle starting on that ellipse will stay on it in accordance with Liouville's theorem. The beam emittance ϵ, i.e. the region in phase space occupied by the beam, gives an upper limit for the size of the ellipse.

When doing calculations and simulations, a matrix formalism is convenient. The change in the deviation u of a particle from one point in the lattice to another is given by

$$\begin{pmatrix} u_f \\ u'_f \end{pmatrix} = \begin{pmatrix} \sqrt{\frac{\beta_f}{\beta_i}}[cos(\psi) + \alpha sin(\psi)] & \sqrt{\beta_i \beta_f} sin(\psi) \\ \frac{\alpha_i - \alpha_f}{\sqrt{\beta_i \beta_f}} cos(\psi) - \frac{1+\alpha_i \alpha_f}{\sqrt{\beta_i \beta_f}} sin(\psi) & \sqrt{\frac{\beta_i}{\beta_f}}[cos(\psi) - \alpha sin(\psi)] \end{pmatrix} \begin{pmatrix} u_i \\ u'_i \end{pmatrix}. \tag{1.7}$$

Because the beam guidance and focusing is performed by applying Lorentz forces, the effect on the particle trajectories depend on the momentum of the particles, and an error in the beam energy (and there is inevitably a spread in energies within the particle beam) will cause a displacement (i.e. a more energetic particle will follow a longer trajectory through the lattice than a less energetic). The particle's final deviation u from the reference trajectory is thus composed of the betatron motion u_β and the dispersion u_δ (i.e. $u = u_\beta + u_\delta$) [12, 19].

Chapter 2

Designing the linac lattice

With more than one pass through the linac and its focusing lattice one inevitably encounters the problem of the beam being focused differently in each pass. This comes as a result of the fact that at $\beta \approx 1$ the focusing from the quadrupoles scales linearly with the energy as

$$f = \frac{\beta E}{egl}. \tag{2.1}$$

Here f is the focal length, β the particles speed and E their energy, g is the quadrupole field gradient and l the quadrupole length [19]. Furthermore, due to the relative change in energy being different in each pass through the linac, the phase advance per cell of the betatron oscillations can not be kept constant in more than one pass and, its rather rapid change in the other passes gives rise to a loss of adiabaticity in the variation of focusing from cell to cell, and results in β-beating. This effect is a real challenge when designing the lattice and makes a conscious choice of the phase advance for thebetatron oscillations essential.

2.1 Choice of phase advance

The phase advance per cell should be chosen so that it stays well away from the critical areas around 0°and 180°, and in particular that it does not come close to these values for a long time. It is also worse to remain in this phase advance region at low energies and this should especially be avoided. We used the computer program Mathematica to study the evolution of the phase advances and to decide what values to use (see figure 2.1). The phase advance per cell ψ is calculated from

$$sin(\psi/2) = \frac{gq}{4p} l_{cell} l_{quad}, \tag{2.2}$$

where q is the charge and p the momentum of the particles in the beam, l_{quad} is the length and g is the field gradient of the quadrupole and l_{cell} is the cell length. A derivation of this formula is given in chapter 3.3.

2.1.1 The 100 GeV and 140 GeV machines

After some qualitative considerations we came to the conclusion that, for the normal recirculating linacs (i.e. the machines without energy recovery), the phase advance can be kept constant in the first pass without this resulting in too much beating in the second [15]. The numbers we ended up using for the simulations were a constant phase advance of 130°in the first pass and an injection energy of

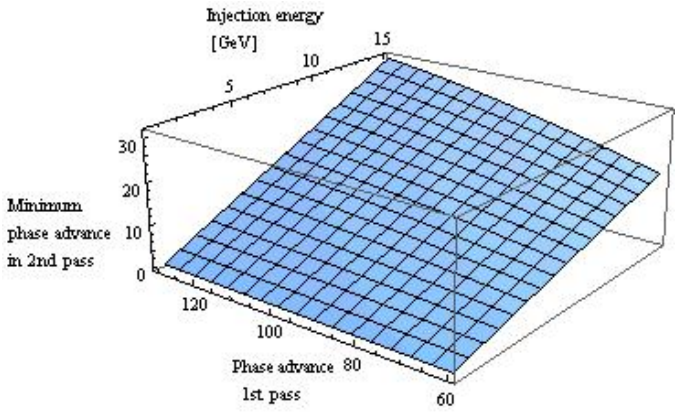

Figure 2.1: The phase advance per cell at the beginning of the second pass through the linac as a function of the phase advance at the beginning of the first pass and of the injection energy. This plot is for a machine with 100GeV collision energy.

5GeV. In the 100 GeV machine the resulting phase advance is 10°at the start of the second pass and 57°at the end. In the 140 GeV machine we have 7°at the start and 56°at the end. Later on we also considered 500 MeV injection energy with the same phase advance of 130°per cell in the first pass, which give 1°phase advance per cell at the beginning of the second pass and 54°at the end in the 100 GeV machine (see figure 2.2), and 0.7°at the start and 54°at the end in the 140 GeV machine.

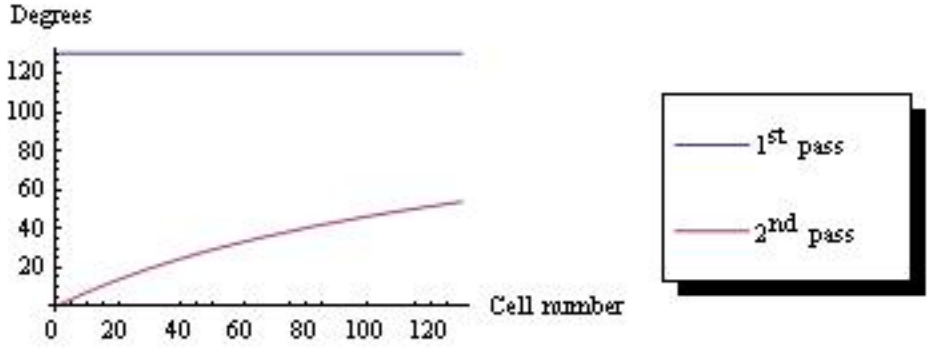

Figure 2.2: The phase advance per cell in both passes through the linac of the RL accelerating from 500 MeV to 100 GeV.

Keeping the phase advance constant in the first pass does obviously not mean that the quadrupole gradient is constant. On the contrary it scales linearly with the beam energy as illustrated by figure 2.3.

2.1.2 The ERL

Designing the lattice for the ERL is inevitably a much bigger challenge than for the normal RLs. Not only do we have two additional passes through the lattice, but these two passes also have a reduction rather than an increase in energy through the linac. For the ERL it is therefore not anymore possible to keep the phase advance per cell constant through the first pass, as this causes a phase advance of

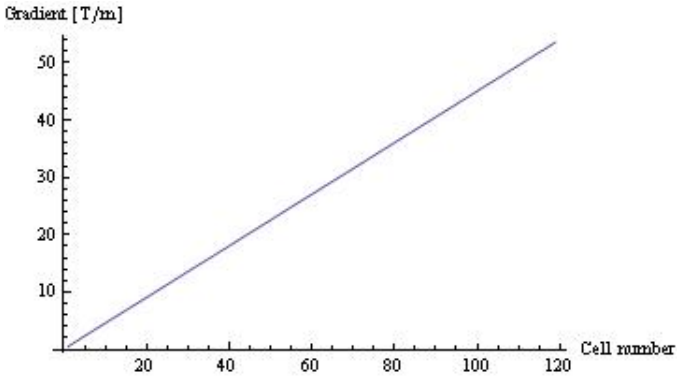

Figure 2.3: The development of the quadrupole gradient through the linac of the RL accelerating from 500 MeV to 100 GeV with a constant phase advance per cell of 130°in the first pass.

180°only half way through the linac in the fourth pass, as shown in figure 2.4. We decided to let the phase advance decrease linearly through the first pass from 130°at the beginning to 30°at the end of the linac. This allowes the beam to be extracted at 13 GeV, a little higher than the injection energy of 5 GeV, and results in a potential energy-recovery efficiency of about 78%.

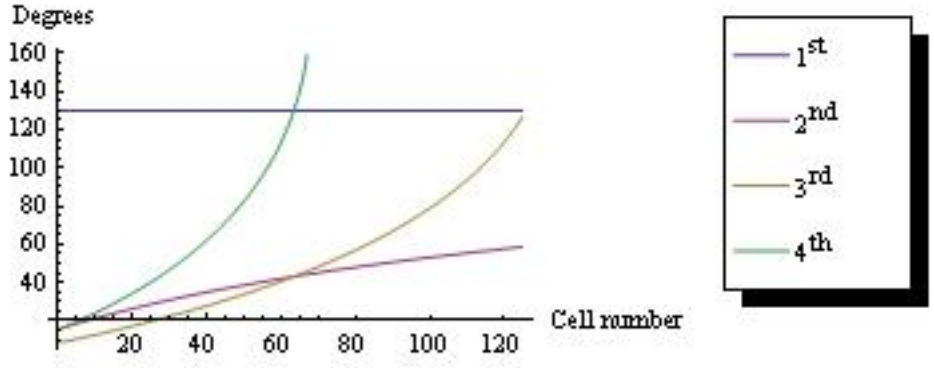

Figure 2.4: The phase advance per cell in each pass through the linac in a 5 to 60 GeV ERL keeping the phase advance constant at 130°per cell in the first pass

Later on, after discussing with several experienced ERL-experts we decided to attempt decelerating the beam all the way down to the injection energy before extraction. And to attempt using a lower injection energy of 500MeV (which was also implemented for the RLs, though the advantages are not as large her as for the ERL). The potential energy recovery efficiency of 99% would increase the luminosity of the machine by a factor of 100 (!) compared to a normal RL. To be able to achieve this the phase advance per cell has to be reduced from 130°at the beginning of the first pass to just 2°at the end (see figure 2.5). The chromatic effects from the large β-amplitude of such a machine might be difficult to control and certainly needs to be studied further (see chapter 6). The development of the gradient is shown in figure 2.6.

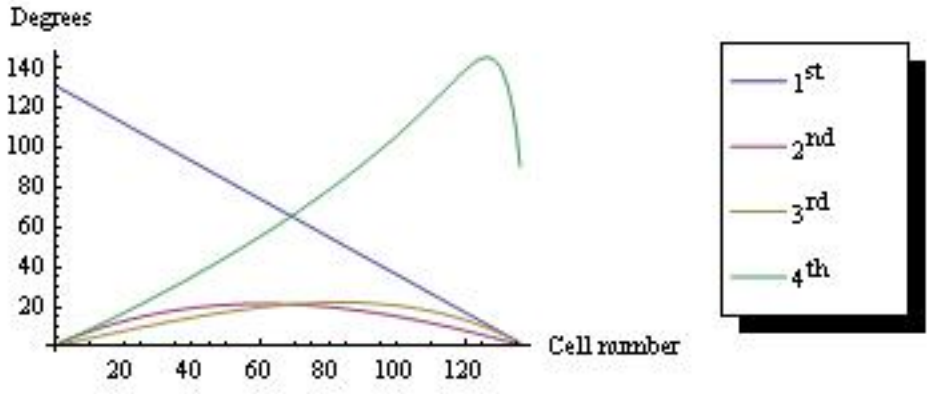

Figure 2.5: The phase advance per cell in each pass through the linac in a 500 MeV to 60 GeV ERL. The phase advance is reduced linearly from 130°to 2°in the first pass. The maximum, and the folling dip in the graph, for the second, third and fourth pass comes as a result of the the phase advance depending on two independent parameters, the beam energy and the quadrupole gradient.

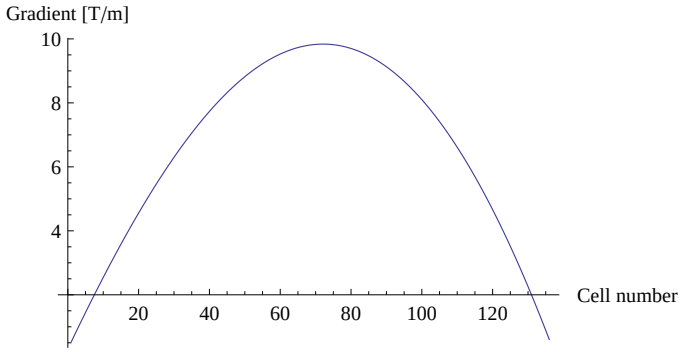

Figure 2.6: The development of the quadrupole gradient through the linac of the ERL accelerating from 500 MeV to 60 GeV and decelerating back to 500 MeV with a phase advance as shown in figure 2.5.

2.2 Placet

Placet is a code to simulate the dynamics of a beam in the main accelerating or decelerating part of a linac. It was developed primarily as a tool for the CLIC project, but turned out to be useful for designing the lattice in the LHeC linac as well. It is written with the script language Tcl [16]. The reason we chose to use Placet, rather than e.g. MAD-X, is that RF-cavities are more accurately simulated in Placet, and later studies will surely need to use Placet, or another program specifically made for linacs, for wake-field and error estimates. We may then make use the files already created for the optics calculations.

The main use of Placet in this work was to calculate the input twiss-parameters for MAD-X at the entrance and exit of the linac, and to cross-check the MAD-X simulations of the twiss-functions in the linac passes. In MAD-X the beam energy is irrelevant for the simulation (it is not even needed as an input parameter) as it is already taken into account in the normalised quadrupole strength, whereas Placet changes the beam's energy as it pass through the cavities and the quadrupole strength are given in energy independent units. Cross-checking the results from the two programs is therefore very useful indeed. An example of atwiss function plot from Placet is shown in figure 2.7.

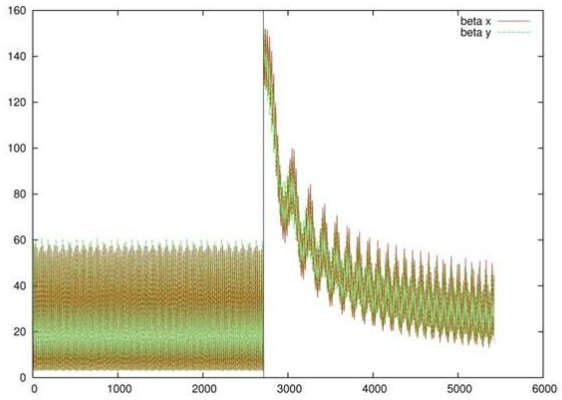

Figure 2.7: Plot of the β-functions in the first and second pass through the linac for a machine accelerating electrons from 5 GeV to 100 GeV simulated using Placet. The two passes are separated by a vertical black line.

Chapter 3

Designing the arc lattice

Previous LHeC ring-linac studies have focused on a race-track design for the RL (see figure 3.1) and this precedent has been followed in this work [17].

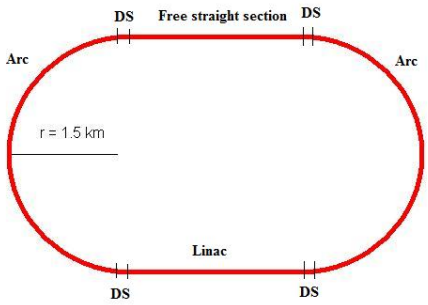

Figure 3.1: Example of the geometry of a race-track RL. DS indicate dispersion suppressors (see chapter 3.4). The radius indicated is the one used in the work presented here.

What is here referred to as the arc consists of the two arc-sections (i.e. sections with dipoles) and one of the straight-sections. The second straight section is the linac. The phase advance per cell is set to 90°everywhere in the arc (see 3.3).

3.1 Choice of radius

There are two correlated effects setting a lower limit on the choice of radius for the arc. These two are power loss due to synchrotron radiation and the growth in emittance from radiation fluctuations. After considering both (only synchrotron radiation losses turns out to be limiting in our case) we chose a radius of 1.5 km for the recirculator, this is large enough for a 140 GeV machine, as we, even if the first linac should be smaller, want to facilitate future upgrades. The effects are briefly explained bellow.

3.1.1 Synchrotron radiation

When charged particles are accelerated they lose part of their energy to electromagnetic radiation. The finite velocity of light gives rise to this effect, qualitatively speaking one could say the electromagnetic-field surrounding the particle fail to

keep up with it and tears itself away. The power of the radiation is calculated from the integral of the Poynting vector $\mathbf{S}$ over a surface enclosing the charge giving

$$P = \int \mathbf{S}\, d\mathbf{A}^* = \frac{2q^2}{3c}\dot{\beta}^{*2}. \tag{3.1}$$

Where q is the charge and $\dot{\beta}^*$ is the acceleration (i.e. the time derivative of the speed β) of the particle in the reference system L^*. Through some manipulations we can express the radiation power in the laboratory reference frame as [19]

$$P = \frac{2q^2}{3c}\gamma^6(\dot{\beta}^2 - [\beta \times \dot{\beta}]^2). \tag{3.2}$$

Decomposing into parts parallel and perpendicular to the propagation we have

$$P_\parallel = \frac{2q^2}{3c}\gamma^6 \dot{\beta_\parallel}^{\,2}, \tag{3.3}$$

$$P_\perp = \frac{2q^2}{3c}\gamma^4 \dot{\beta_\perp}^{\,2}. \tag{3.4}$$

We also know that the accelerating force in each direction is given by

$$\mathbf{F}_\parallel = \frac{d\mathbf{p}_\parallel}{dt} = \gamma^3 mc\beta_\parallel, \tag{3.5}$$

and

$$\mathbf{F}_\perp = \frac{d\mathbf{p}_\perp}{dt} = \gamma mc\beta_\perp. \tag{3.6}$$

Using this we now see that the power of radiation caused by acceleration parallel to the direction of propagation is independent of the energy of the particle and only depends on the accelerating force working on it. Acceleration in the direction perpendicular to the direction of propagation on the other hand causes radiation with power proportional to the square of the energy of the particle. This radiation, known as synchrotron radiation, is very important in particle accelerators. An accelerator with a circular trajectory of radius ρ and circulating a particle with energy E has power loss from synchrotron radiation given by

$$P_\gamma = \frac{2q^2\beta^4 E^4}{3m^4c^7\rho^2}. \tag{3.7}$$

When the particle is an electron we may simplify to

$$P_\gamma = \frac{2e^2\beta^4 E^4}{3m_e^4c^7\rho^2} = \frac{cC_\gamma E^4}{2\pi\rho^2}, \tag{3.8}$$

where C_γ indicates Sands radiation constant for electrons defined as

$$C_\gamma = \frac{4\pi r_c}{3(m_e c^2)^3} = 8.8575 \times 10^{-5}\frac{m}{GeV^3}. \tag{3.9}$$

The loss of energy per turn (with $\beta \approx 1$) is

$$\Delta E = C_\gamma \frac{E^4}{\rho^2}. \tag{3.10}$$

The synchrotron radiation losses should as a rule of thumb not exceed 1% of the energy of the machine [20]. In a 140 GeV RL with two passes, the particles passing through the arc at 70 GeV, this requires a radius of 1.5 km.

3.1.2 Radiation fluctuations and emittance growth

When considering the synchrotron radiation loss it is natural and unproblematic to disregard the quantum property of the radiation (as we are only interested in the average energy loss per turn). However, the fact that the radiation is quantised has an important effect on the beam, that also put requirements on the geometry of the machine. We can get a qualitative understanding of the effect by considering that each particle has a certain probability of emitting a photon at any given time as it passes through the dipoles of the arc and is accelerated inwards, orthogonal to its trajectory. Particles initially having similar position and energy may thus lose different amounts of energy, and lose it at different times, causing them to follow slightly different trajectories and resulting in emittance growth in the beam [14]. The growth in normalised emittance $\Delta\gamma\epsilon_x$ (the physical emittance is indicated by ϵ and $\gamma = E/m_0$ is the gamma-function of the particles) of a beam with energy E and following a trajectory with radius ρ, is calculated from

$$\Delta\gamma\epsilon_x = 6.2 \times 10^{-5} \frac{E^6}{\rho D^3} F, \tag{3.11}$$

where D is the number of dipoles the beam passes through and F is a numerical factor controled by the lattice design. For a lattice consisting of FODO-cells with 90°phase advance per cell, we have

$$F = 2.50 \frac{l_{cell}}{l_{dipole}}, \tag{3.12}$$

where l_{cell} is the length of the cell and l_{dipole} the combined length of the dipoles in the cell [18]. In this paper the FODO-cells are 24 m with two dipoles of 9.8 m (see chapter 5.1 for further details).

Using the radius we obtained from considerations of the synchrotron radiation of 1.5 km, in an arc consisting of 480 cells with 960 dipoles, and 140 GeV particle energy at the collision point (which was also used for the synchrotron radiation considerations), i.e. about 70 GeV during the passage through the arc, we get a growth in normalised emittance of about 20 μ m. To get as efficient collisions as possible in the LHeC, the geometric emittance of the electron beam should be of the same order of magnitude as the emittance of the proton beam in LHC. Although we would get a higher luminosity with smaller beam size of the electron beam, too small a beam size will have a destabilising effect on the proton bunches and possibly destroy them. The normalised beam emittance in the LHC in nominal operation will be 3.75 μ m which at 7 TeV energy means a physical emittance of 5×10^{-10} m [10]. Taking about half of this for the emittance in the electron beam, and looking first at the 100 GeV machine (as emittance shrinks with increasing energy), we find that this requires a normalised emittance of about 50μ m. This emittance should be easily obtainable using conventional technology for the injector (at least for the electrons; as mentioned before the positron supply is difficult, but that is another story altogether). Sustaining the parameters used before for the arc (i.e. 1.5 km radius and 480 cells), the growth in normalised emittance from radiation fluctuations becomes 3 μ m which is small enough to be disregarded. Using the same normalised emittance of 50μ m in the 140 GeV machine, and adding the 20μ m from radiation fluctuations we get a physical emittance of 2.5×10^{-10} m and so everything works out very well and we use these parameters for the design.

3.2 MAD-X

MAD-X is a general purpose accelerator and lattice design program developed for the design of the LHC from the previously existing program MAD-8 (that was also developed at CERN) [11]. It is not optimized for the design of linacs, but can be put to this use as well and, as the linac designs being discussed for the LHeC ring-linac option are recirculating, it was decided that MAD-X would be the most practical program choice for the lattice design, complemented with computations from Placet. MAD-X is also an advantageous choice because of the abundance of people working at CERN using the program with enormous skill. In addition to calculating peridodic solutions for the twiss-functions, MAD-X can also be used to match the lattice, by adjusting a certain choice of input parameters (e.g quadrupole strength, drift length, etc.), to obtain a given set of beam parameters locally, i.e. in a particular position, or globally. An example of a twiss function simulated with MAD-X is shown in figure 3.2.

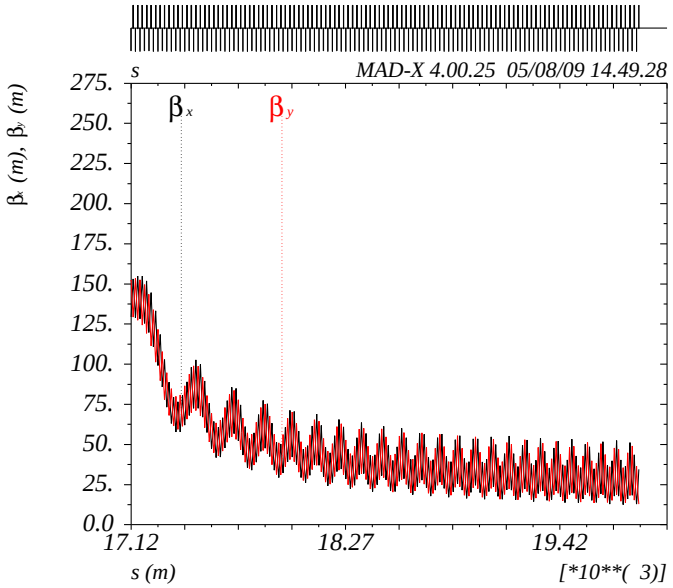

Figure 3.2: The twiss functions in the second pass through the linac for a machine accelerating electrons from 5 GeV to 100 GeV simulated using MAD-X. Comparing this plot with one made using Placet (see figure 2.7) shows that the two programs give approximately the same function.

3.3 Matching to 90°phase advance

As previously mentioned we want a 90°phase advance per cell in the arc (i.e. in the linac-less straight section and both arc sections). This is the natural choice as it is in the middle of the allowed phase advances, not causing the twiss-functions to grow uncontrollably, and, as no particular reason suggests diverting from it, we stick to this value. It is easy to find a good approximation for what quadrupole strength that give this phase advance by making use of the general transfer matrix M (see

chapter 1.3) over β-function period (i.e. with $\beta_i = \beta_f$), expressed as a function of the Twiss parameters α, β and γ and the phase advance ψ

$$M = \begin{pmatrix} cos(\psi) + \alpha sin(\psi) & \beta sin(\psi) \\ -\gamma sin(\psi) & cos(\psi) - \alpha sin(\psi) \end{pmatrix}, \tag{3.13}$$

and the matrix for a complete FODO-cell in thin-lens approximation,

$$M_{FODO} = \begin{pmatrix} 1 - \frac{l_{cell}^2}{8f^2} & \frac{l_{cell}}{2}(1 + \frac{l_{cell}}{4f}) \\ \frac{l_{cell}^2}{16f^3} - \frac{l_{cell}}{4f^2} & 1 - \frac{l_{cell}^2}{8f^2} \end{pmatrix}. \tag{3.14}$$

Comparing (3.13) and (3.14), and using that $trace(M) = 2cos(\psi)$, gives

$$cos(\psi) = \frac{1}{2}cos(\psi) = 1 - \frac{l_{cell}^2}{8f^2}. \tag{3.15}$$

We make the replacement $1/f = kl$, where l is the length of the quadrupole and k is an energy independent representation of the strength of the quadrupole, henceforth referred to as the k-value, defined as $k = gq/p$, where q is the charge and p the momentum of the particles in the beam and g is the field gradient of the quadrupole. After some trigonometric manipulation this results in [12]

$$k = \frac{4sin(\psi/2)}{l_{cell}l_{quad}}. \tag{3.16}$$

With our parameters (i.e. $\psi = 90°$, $l_{cell} = 24m$ and $l_{quad} = 470mm$), this gives the k-value $0.250747/m^2$ for 90°phase advance. However, to get exactly the phase advance we want, and avoid the small change of the twiss-functions caused by the focusing effect of the dipoles in the arcs, we use the mathcing command in MAD-X. This is done separately for a FODO-cell with and without dipole, as well as with the half-dipole used in the dispersion suppressor, and we find slightly different values for the quadrupole strengths than what we calculated from (3.16). The final k-values, that are used in the arcs for all design options (note that, although the quadrupole gradient is not, the k-value is energy dependent), are $0.254091/m^2$ in both planes in cells without dipoles, $0.254081/m^2$ for quadrupoles focusing in the horizontal plane and $-0.254089/m^2$ for quadrupoles defocusing in the horizontal plane in cells with dipoles, and $0.254088/m^2$ for focusing and $-0.254090/m^2$ for defocusing quadrupoles (still in the horizontal plane) in cells with half-dipoles (i.e. in the dispersion suppressor). To find the gradient g of the quadrupole (i.e. the physical parameter that is needed for constructing and calibrating the magnets) we use the definition of the k-value.

3.4 The dispersion suppressor

Passing the beam through the arcs obviously produces dispersion and, as we would like to avoid having dispersion in the straight sections (especially where we have the linac) we want to bring the dispersion and its derivative to zero before and after the arc. An elegant way of doing this, provided that the required space is available, is by using a dispersion suppressor. This method makes use of the fact that the dispersion function is periodic (true provided that the lattice is periodic) which enables us to stop the oscillation of the dispersion function at zero by reducing the strength of the dipoles at the beginning and end of the arc. One makes use of two FODO-cells and reduces the strength of the dipoles to a fraction, the size of which depends on the phase advance in the cells. In the case of a 90°phase advance per cell the strength should be set to 50% of the standard dipole for all dipoles in both

cells. The dispersion suppressor based on varying the dipole strength has the advantage of not causing a change in the beta-function, or only changing it very little and in a way easily compensated by slight adjustments of the quadrupole strength in the cells concerned, as opposed to the most obvious alternative method of manipulating the dispersion entirely with the focusing magnets [19]. After obtaining a dispersion of approximately zero in all of the straight section using this standard method we used the MAD-X matching function to get exactly zero dispersion by tuning the dipole strengths slightly. The dispersion function and the β-functions in an LHeC dispersion suppressor (this actually looks similar in all proposals discussed in this paper) is shown in figure 3.3.

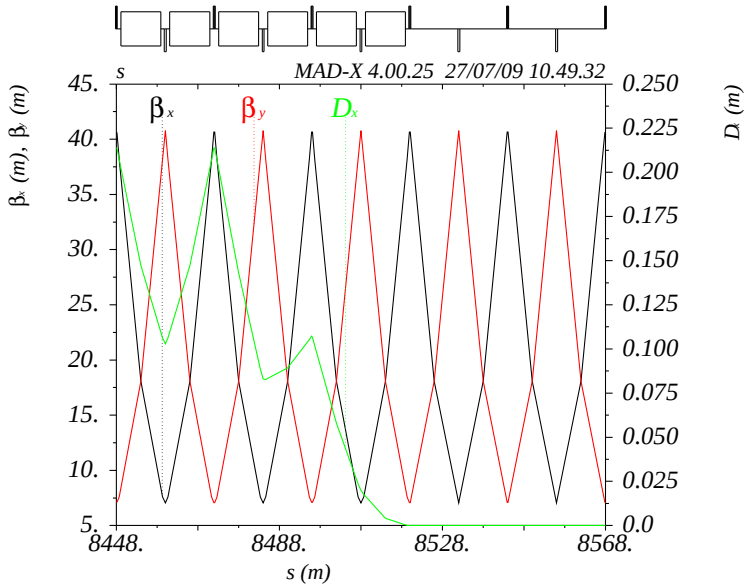

Figure 3.3: Example of the β-functions and dispersion function in a dispersion suppressor. This particular dispersion suppressor is from the machine accelerating from 5 GeV to 100 GeV, but it looks similar in all of the designs (although the β-functions might look different if the plot also shows the transition region (see chapter 4).

Chapter 4

Putting it all together; or, the transition region

After finding a working lattice for both linac and arc the next challenge is putting the two together. Simply placing the arc at the end of the linac without any further adjustments will, because of the large difference in betatron amplitude, not work. To change the twiss parameters from the matched values at the end of the linac to the matched values at the begining of the arc (or similarly the other way around, i.e. from the arc to the linac) we introduce two cells between the linac and arc and let the strength of the quadrupoles in these cells be variables in the match command of MAD-X. The input parameters are the twiss parameters calculated in simulations of the arcs and linacs separately.

4.1 The 100 GeV and 140 GeV machines

For the first pass through the linac of the 100 GeV and 140 GeV machines it is relatively easy to connect to the arc. As the phase advance is kept constant at 130°, the change to 90°can be done in the two cell transition region without causing any serious distortion of the β-functions. A plot of this transition region (which is similar for all the RL machines) is shown in figure 4.1.

The second transition region is different for each of the machines. Although we do get a peak in the β-function of the 5 to 100 GeV machine, it is relatively moderate, and does probably not create uncorrectable chromatic effects. This transition region is shown in figure 4.2.

In the machines with 500 MeV injection energy the β-function peaks are much larger and these designs might need some further work (see chapter 6). The 500 MeV to 140 GeV machine in particular, has a challenging second transition region, as can be seen in figure 4.3.

4.2 The ERL

The ERL designs do, contrary to the RL designs, not have any easily constructed transition regions. As the phase advance is not kept constant in the first pass even the first transition region needs to perform a considerable adjustment of the β-functions. And the β-beating, that is now present in all the linac passes, causes the adjustment to be even bigger. In the machine beginning the acceleration at 5 GeV and ending the deceleration at 13 GeV the resulting twiss functions are probably

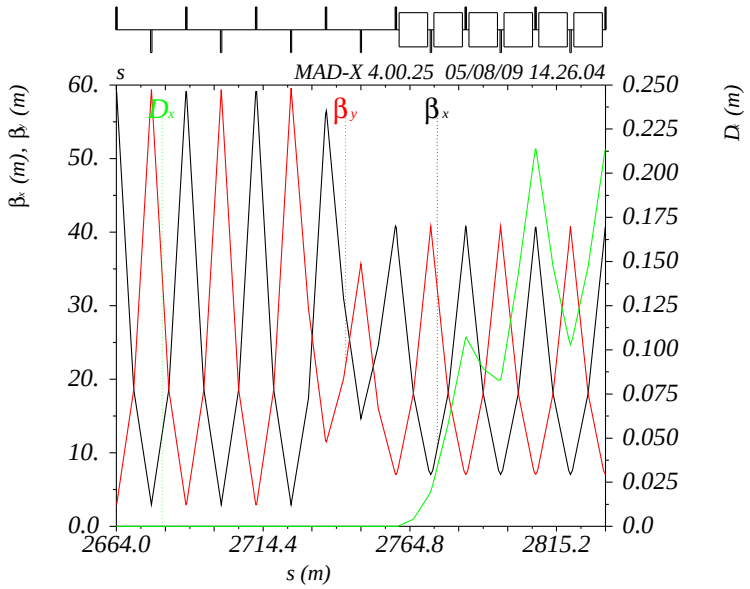

Figure 4.1: Plot of the horizontal (β_x) and vertical (β_y) β-function and the dispersion function (D_x) in the first of two transition regions in the 100 and 140 GeV machines, where the phase advance is changed from 130°to 90°. The cell structure is indicated above the plot.

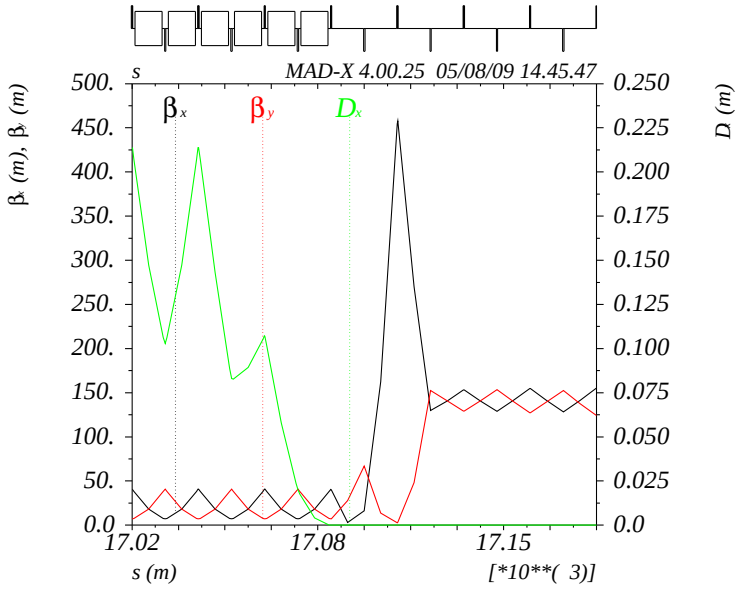

Figure 4.2: Plot of the horizontal (β_x) and vertical (β_y) β-function and the dispersion function (D_x) in the second and last of the two transition regions in the 5 to 100 GeV machine. The phase advance is changed from 90°to 10°(see chapter 2.1.1) and we get a peak of 458 m in the horizontal β-function.

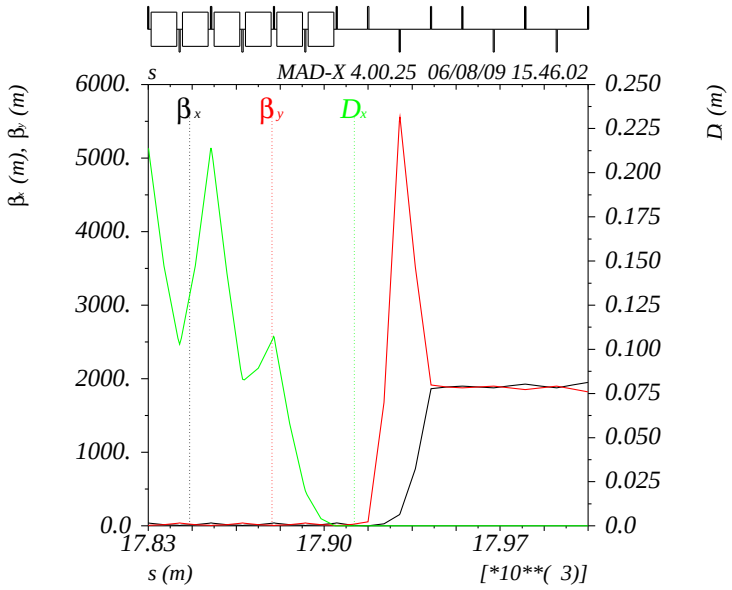

Figure 4.3: Plot of the horizontal (β_x) and vertical (β_y) β-function and the dispersion function (D_x) in the second of two transition regions in the 500 MeV to 140 GeV machine. The phase advance is changed from 90°to 0.7°(see chapter 2.1.1) and we get a peak of 1977 m in the horizontal and 5555 m in the vertical β-function. Note also that two consecutive quadrupoles focus in the same direction indicating the difficulty of this transition.

tolerable, with a maximum of the β-function at 524 m in a transition region structured as in the RL designs, i.e. with two normal sized cells. However, the machine accelerating from and decelerating to 500 MeV is much more challenging, requiring cells with double size (i.e. 48 rather than 24 m) in the third and fifth (see figure 4.4) transition regions and giving maximum β-values of 7666 m in the horizontal and 2006 m in the vertical plane.

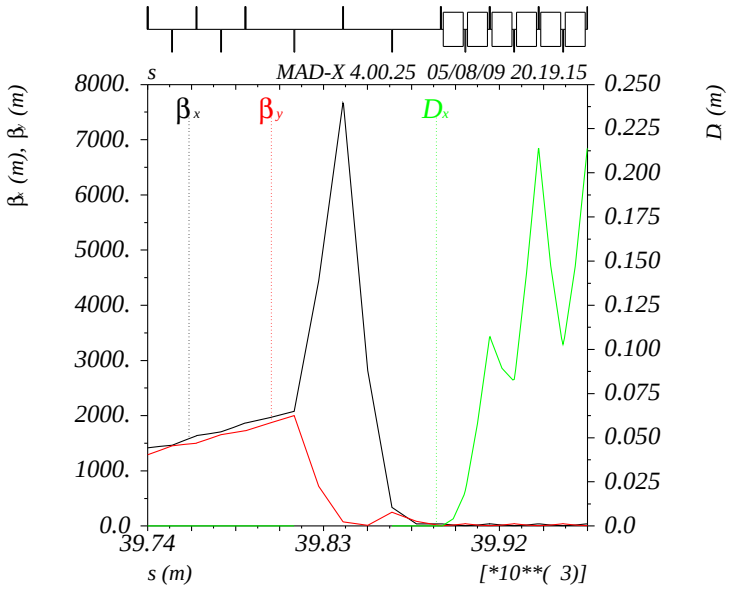

Figure 4.4: Plot of the horizontal (β_x) and vertical (β_y) β-function and the dispersion function (D_x) in the fifth of six transition regions in the 500 MeV to 60 GeV ERL. The phase advance is changed from 1.9°to 90°(see chapter 2.1.1) and we get a peak of 7666 m in the horizontal and 2006 m in the vertical betatron amplitude. Note that here the cells in the transition region have twice the normal cell size.

Chapter 5

Results: Optics for the linac options for LHeC

In this chapter the final results are presented. First some general parameters are given (general meaning that they are the same for all machine designs in this paper) and then each of the three design options is discussed separately.

5.1 Some general parameters

The basis for all the designs is the standard FODO-cell (see figure 1.5), which as the most simple realistic periodic lattice structure and therefore a natural choice (at least for the first attempt). The cell length is $24m$ (except in the second and fifth transition region in the 500 MeV to 60 GeV ERL where it is $2 \times 24m = 48m$ due to longer drift spaces (see chapter 4.2), the same as in the European X-Ray Free-Electron Laser (XFEL) currently under construction at DESY in Hamburg [8]. The quadrupoles are 470 mm long everywhere in the machine, which gives a feasible requirement for the gradients of the quadrupoles (the maximum gradient being 78 T/m at the end of the 140GeV linac) [20]. This means the quadrupoles are separated by 11.53 m that can accommodate RF-cavities or dipoles, as well as other necessary equipment for beam diagnostics (e.g. beam position monitors) or error correction (e.g.sextupoles).

All dipoles are 9.8 m long which is a more or less randomly chosen number, but not far from the maximum of what we can fit between the quadrupoles. If it turns out to be more practicable there should be no problem splitting this into two or more smaller dipoles. The length of the RF-cavities is set to 8.4 m, following similar considerations as for the dipoles, but leaving some more free space for other instruments that may be required. The RF-cavities might also have to be partitioned up (both XFEL and the current design for ILC does for instance have cavity structures of about one meter [8, 9]). The necessary gap between the separate components will in this case take up some of the free space.

The radius of the recirculating arc is 1.5 km and the initial normalised emittance from the injector is set to 50μ m for all the designs (see chapter 3.1). Other parameters, not directly affecting the lattice design, like bunch spacing, beam current, etc., are not discussed here.

5.2 Optics for a 100 GeV RL

The 100 GeV RL is the most moderate of the machine designs and the parameters are throughout chosen close to, or within the scope of, what can be done with conventional technology today. The accelerating gradient is 25 MV/m, only slightly more than in the XFEL, which is to be operating at 23.6 MV/m, and much smaller than the 32 MV/m projected for the ILC [8, 9].

5.2.1 Starting at 5 GeV

Figure 5.1 shows the β-functions for the machine accelerating the electrons from 5 to 100 GeV. The total length of the linac (i.e. the part with accelerating cavities) is 2712 m and it consists of 113 cells.

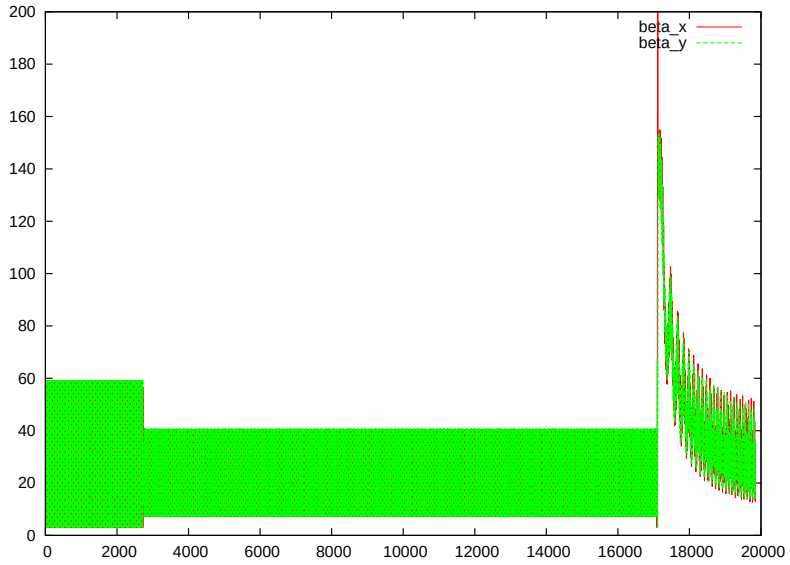

Figure 5.1: Plot of the β-functions for a machine accelerating electrons from 5 GeV to 100 GeV with two passes through the linac (the lattice is the same for both passes in the linac). The graph is somewhat cropped, excluding some spikes of the β-function in the transition region (i.e. the region between the linac and the arc), to give a better view of the function in the other parts of the machine. The maximums of the β-functions are 458 m in the horizontal (β_x) and 154 m in the vertical (β_y) plane, both these values are reached in the transition region (see chapter 6 for discussion about the spikes in the transition regions).

5.2.2 Starting at 500 MeV

Figure 5.2 shows the β-functions for the machine accelerating the electrons from 500 MeV to 100 GeV. The total length of the linac is 2856 m and it consists of 119 cells.

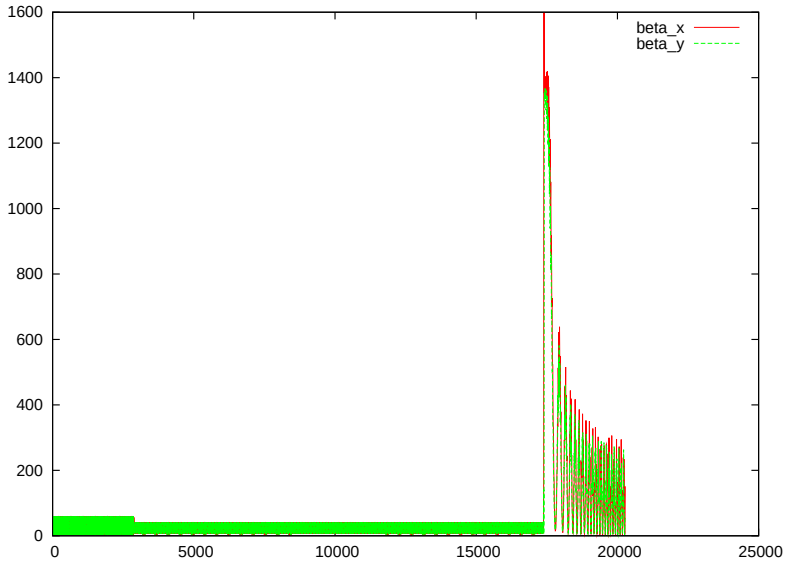

Figure 5.2: Plot of the β-functions for a machine accelerating electrons from 500 MeV to 100 GeV with two passes through the linac. Like in figure 5.1 the graph is cropped. The maximums of the β-functions are reached in the transition region and are 4304 m in the horizontal (β_x) and 1367 m in the vertical (β_y) plane (see chapter 6 for discussion).

5.3 Optics for a 140 GeV RL

To reduce the length of the 140 GeV RL somewhat we assume an accelerating gradient equal to the ILC gradient of 32 MV/m. This makes the linac 3120 m with 130 cells. As the simulations for the 140 GeV RL were done after the decision to use 500 MeV injection energy, these were the only simulations done (although preliminary calculations and simulations were done with 5 GeV injection energy as well). The β-functions are shown in figure 5.3.

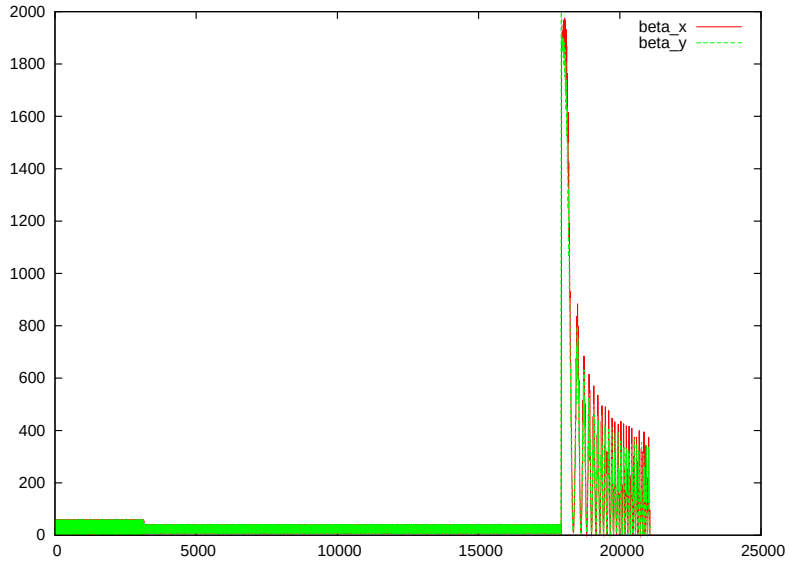

Figure 5.3: Plot of the β-functions for a machine accelerating electrons from 500 MeV to 140 GeV with two passes through the linac. Like in figure 5.1 the graph is cropped. The maximums of the β-functions are reached in the transition region and are 1977 m in the horizontal (β_x) and 5555 m in the vertical (β_y) plane (see chapter 6 for discussion).

5.4 Optics for a 60 GeV ERL

As mentioned in the introduction it will probably be necessary to run in the ERL in continuous wave (cw) mode. And as this increases the dependence of the heat loss (and thus of the power demand of the cryogenics system) on the accelerating gradient we are forced to reduce this somewhat. We decided to run with 13 MV/m for which the cryogenics costs are still reasonable [3]. The XFEL scheme for running in cw-mode operates with a gradient of 7.5 MV/m [8].

5.4.1 Starting at 5 GeV

Figure 5.4 shows the β-functions for the machine accelerating the electrons from 5 GeV to 60 GeV and decelerating to 13 GeV. The total length of the linac is 3000 m and it consists of 125 cells.

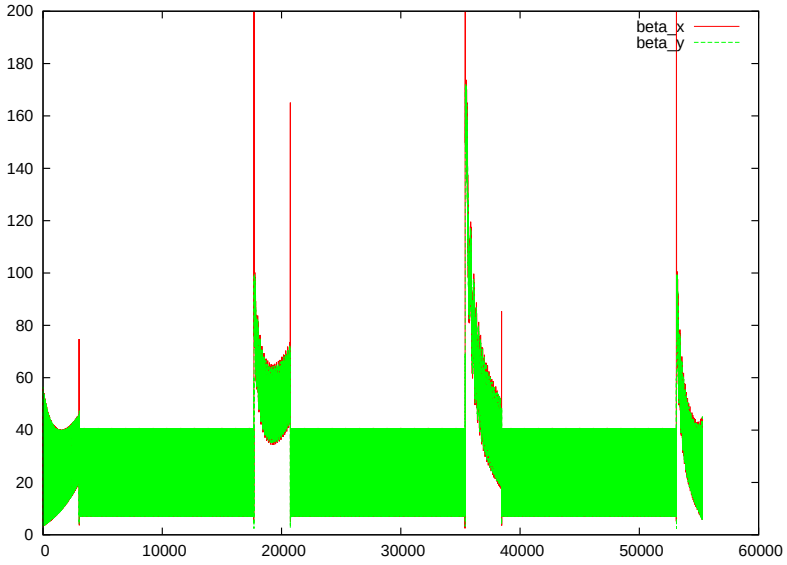

Figure 5.4: Plot of the β-functions for a machine accelerating electrons from 5 GeV to 60 GeV with two passes through the linac and decelerating back to 13 GeV with two more passes through the same linac, but extracting the particles after 2160 m of the second pass of deceleration. Like in figure 5.1 the graph is cropped. The maximums of the β-functions are reached in the transition region and are 524 m in the horizontal (β_x) and 172 m in the vertical (β_y) direction (see chapter 6 for discussion).

5.4.2 Starting at 500 MeV

Figure 5.5 shows the β-functions for the machine accelerating the electrons from 500 MeV to 60 GeV and decelerating all the way back to 500 MeV. The total length of the linac is 3264 m and it consists of 136 cells.

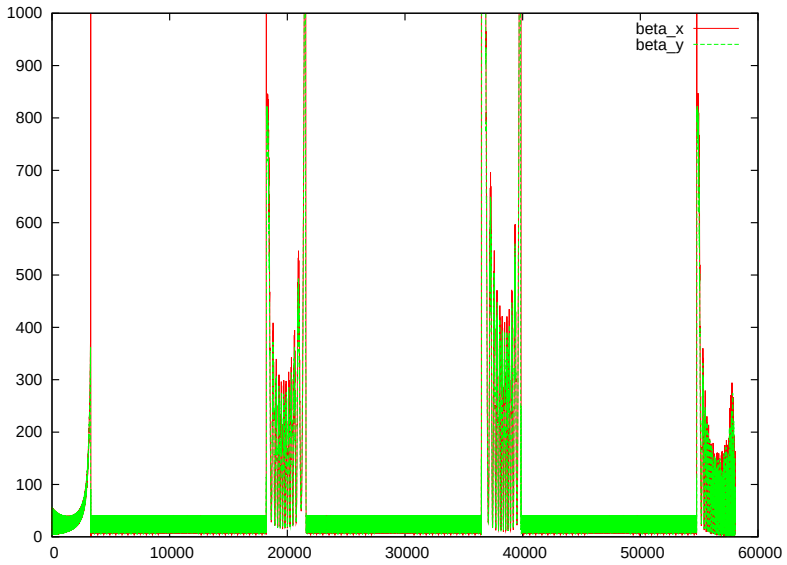

Figure 5.5: Plot of the β-functions for a machine accelerating the electrons from 500 MeV to 60 GeV with two passes through the linac and decelerating back to 500 MeV with two more passes through the same linac. Like in figure 5.1 the graph is cropped. The maximums of the β-functions are reached in the transition region and are 7666 m in the horizontal (β_x) and 2006 m in the vertical (β_y) direction (see chapter 6 for discussion).

Chapter 6

Conclusion

The work presented in this report have demonstrated the feasibility of a recirculating linac scheme for the LHeC with 100 or 140 GeV collision energy or 60 GeV collision energy with energy recovery, and presented a possible lattice for each of these machines. Several tasks do remain however, also concerning the lattice design.

The next step should probably be to track a beam through the lattice using MAD-X to verify that the analytical estimate of the emittance growth (calculated from (3.11)) is correct, to observe the effect on the emittance from the energy spread introduced through the cavities (which first have to be included in the MAD-X files) and to observe the chromatic effects. The chromatic effects are very likely to be large because of the high peaks in the transition regions between the linac and the arcs. This is in particular a problem in all the machines with 500MeV injection energy where the peaks are enormous and will almost certainly cause problems. One can attempt to reduce the chromatic effects by chromatic correction with sextupoles, but it might be necessary to make changes to the lattice to reduce the peaks, e.g. by increasing the drift space between the quadrupoles in the transition region.

Other tasks for the future are to study the wake-field effects in the linac (it will probably be most practicable to use Placet for this; the lattice files already made to calculate the twiss functions can then be used) and higher order mode heat losses.

6.1 Acknowledgements

This work has been done in close colaboration with Frank Zimmermann, my supervisor at CERN, that, in addition to giving invaluable help and guidance to the actual work, made me feel welcome and at home in a new institution, city and country. My office mate Frank Stulle has been very helpful and forthcoming on all occasions, made sure I always had company for lunch, answered questions about computer programs, magnet lengths and wine festivals and showed great patience when I now and then misplaced my office key. Barbara Dalena and Daniel Schulte deserve thanks for their introduction to and assistance with the computer program Placet, and I would also like to thank my supervisor at NTNU, Bo-Sture Skagerstam that made it possible to do the project work at CERN and somewhat differently than what is ordinary. Lastly I would like to thank Rossana, Timo, Alberto, Silvia, Eduard, Cristina, Claudio, Paolo, Lorenzo and Marcus for including me in the St. Genis family and making my stay at CERN a beautiful experience.

Bibliography

[1] O. Bruning. "Summary of the accelerator working group". LHeC workshop in Divonne, September 2008.

[2] F. E. Close. Rapporteur talks at Singapore (deep inelastic scattering) and at Hadron 90 (conference summary). *Nucl Phys B (Proc Suppl)*, 21:423–429, 1991.

[3] A. Eide. "Electrical power of ring-linac option for LHeC". Project report from EPFL, 2008.

[4] F. Zimmermann et al. Linac-LHC ep collider options. *Proc. of EPAC08*, pages 2847–2849, 2008.

[5] F. Zimmermann et al. The Large Hadron-electron Collider (LHeC) at the LHC. *Proc. of PAC09*, 2009.

[6] J. Dainton et al. Deep inelastic electron-nucleon scattering at the LHC. *JINST*, 1, 2006.

[7] J. Dainton et al. Prospects for a Large Hadron-electron Collider at the LHC. *Proc. of EPAC08*, pages 1903–1905, 2008.

[8] M. Altarelli et al. *The Technical Design Report of the European XFEL*. DESY, 2007.

[9] N. Walker et al. *International Linear Collider Reference Design Report Volume 3*. ILC, 2007.

[10] O. Bruning et al. *LHC Design Report Volume I*. CERN, 2004.

[11] W. Herr and F. Schmidt. A MAD-X primer. *CERN-AB-Note-2004-027*, 2004.

[12] B. J. Holzer. Lattice design in high-energy particle accelerators. *CERN-2006-002*, pages 31–74, 2003.

[13] M. Klein and P. Newman. LHeC: novel designs for electron-quark scattering. *CERN Courier*, 2009.

[14] M. Sands. *The Physics of Electron Storage Rings - An Introduction*. SLAC, 1970.

[15] D. Schulte. Private communication.

[16] D. Schulte. Placet: A program to simulate drive beams. *CERN-CLIC-Note-437*, 2000.

[17] J. Skrabacz. Optimizing cost and minimizing energy loss in the recirculating race-track design of the LHeC electron linac. *CERN-AB-Note-2008-043*, 2008.

[18] L. C. Teng. Minimizing the emittance in designing the lattice of an electron storage ring. *Fermilab-TM-1296*, 1984.

[19] H. Wiedemann. *Particle Accelerator Physics*. Springer, 1998.

[20] F. Zimmermann. Private communication.